Journal Pre-proofs

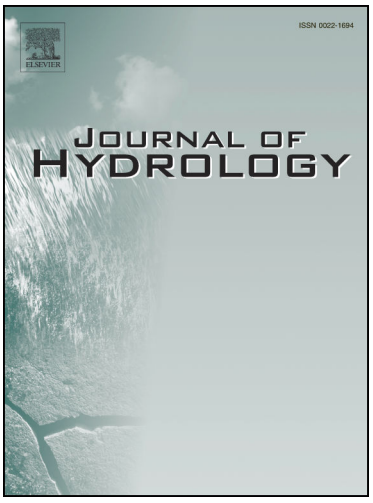

Research papers

Vertical Water Age and Water Renewal in a Large Riverine Reservoir

Bo Gai, Bertram Boehrer, Jian Sun, Yuanyi Li, Binliang Lin, Tom Shatwell

PII: S0022-1694(24)00095-7
DOI: https://doi.org/10.1016/j.jhydrol.2024.130701
Reference: HYDROL 130701

To appear in: *Journal of Hydrology*

Received Date: 1 November 2023
Revised Date: 3 December 2023
Accepted Date: 12 December 2023

Please cite this article as: Gai, B., Boehrer, B., Sun, J., Li, Y., Lin, B., Shatwell, T., Vertical Water Age and Water Renewal in a Large Riverine Reservoir, *Journal of Hydrology* (2024), doi: https://doi.org/10.1016/j.jhydrol.2024.130701

Vertical Water Age and Water Renewal in a Large Riverine Reservoir

Bo Gai [1, 2], Bertram Boehrer [2], Jian Sun [1, *], Yuanyi Li [3], Binliang Lin [1], Tom Shatwell [2]

[1] State Key Laboratory of Hydroscience and Engineering, Department of Hydraulic Engineering, Tsinghua University, Beijing, China

[2] Department of Lake Research, Helmholtz Centre for Environmental Research (UFZ), Magdeburg, Germany

[3] School of Marine Science and Technology, Tianjin University, Tianjin, China

*Corresponding author.

Email addresses:

bo.gai@ufz.de/gb17@mails.tsinghua.edu.cn (B. Gai),

bertram.boehrer@ufz.de (B. Boehrer),

jsun@mail.tsinghua.edu.cn (J. Sun),

liyuanyi@tju.edu.cn (Y. Li),

linbl@mail.tsinghua.edu.cn (B. Lin),

tom.shatwell@ufz.de (T. Shatwell).

*Current address: State Key Laboratory of Hydroscience and Engineering, Department of Hydraulic Engineering, Tsinghua University, Beijing, China

Abstract

Water quality and hypoxia in lakes and reservoirs are strongly associated with water renewal. Yet vertical water exchange is still not fully understood and challenging to evaluate in highly dynamic systems. Here, we applied a scaling approach using the vertical timescale, vertical water age (*VWA*), defined as time since a water parcel last touched the water surface. We established a 3D hydrodynamic-based age model to quantify the vertical water renewal in Xiangxi Bay, a tributary bay of the Three Gorges Dam. The integrated effects of hydrodynamic processes like stratification, intruding density currents from the mainstream and upstream inflow on the vertical renewal were accounted for. Results indicated that the spatial-temporal distribution of *VWA* in Xiangxi Bay depended on stratification and forms of intruding density currents. Age was large in spring and summer, and small in autumn and winter, reaching a maximum of 25 days in April. The vertical water renewal was faster during bottom intrusions from the mainstream than during middle and surface intrusions. At times, the epilimnion contained old water due to circulations, and the hypolimnion contained young water due to upstream flushing. In contrast to natural lakes, the bottom water was often younger than overlying intermediate waters. This demonstrated that mixed layer depth was insufficient to fully capture the vertical exchange in riverine systems with significant surface/bottom intrusion. The findings suggested *VWA* as a quantitative measure of vertical water transport in highly dynamic systems and its usability for environmental water management.

Keywords: vertical water renewal, water age, thermal stratification, hypoxia, 3D hydrodynamic-based age model, water environmental management

1 Introduction

Water renewal in the vertical direction in free-surface waterbodies is of central importance for the ecology of freshwater systems. Vertical water renewal, which includes both water mixing and advection processes, replenishes the deep water with oxygen, releases accumulated gases from decomposition processes, and distributes all kinds of nutrients in the water column. An insufficient vertical renewal can hamper recharge of deep water with oxygen, causing hypolimnetic oxygen depletion (Muller et al., 2012, Bocaniov et al., 2020), and subsurface oxygen minima (Wentzky et al., 2019), facilitating the accumulation of dissolved gases and metabolic substances, e.g. carbon dioxide or methane in the deep water (Boehrer et al., 2017, Horn et al., 2017). It can also provide favourable conditions for phytoplankton concerning density gradient, light availability and nutrient supply. Algal blooms can be the consequence (O'Brien et al., 2009). Vertical renewal and mixing move phytoplankton cells through the exponentially changing underwater light field and determine their light exposure, ultimately influencing primary production rates (Shatwell et al., 2012, Köhler et al., 2018). Furthermore, the supply of deeper nutrients to the photic zone (Dong et al., 2019), and the transformation and consumption of organic matter (Xiong and Shen 2022), which are major components of internal loading, are closely related to water vertical renewal.

Pollution, eutrophication, and hypoxia are ubiquitous in inland waters with low water exchange when there is an overabundance of nutrients and organic matter (Curtis et al., 2011, Holbach et al., 2014). The filling of the Three Gorges Reservoir (TGR) in June 2003 altered the natural connectivity and hydrodynamic processes in the fluvial system fundamentally. For instance, flow velocity decreased, turbulent mixing weakened and residence time increased. Each of these changes could affect water renewal seriously. Indeed, water quality has deteriorated in the reservoir, with intense algal blooms (Liu et al., 2012) and hypoxia (Ji et al., 2022) occurring in some tributary bays and threatening drinking water security for residents in the TGR region (Ministry of Environmental Protection of China 2014). Accordingly, the effect of dam operation on water renewal has gained increasing attention in TGR (Li et al., 2020b) and many other reservoirs worldwide (Wu et al., 2017, Stephens et al., 2020). Water renewal in both vertical and horizontal directions is crucial for reservoir self-purification and self-restoration (Liu et al., 2013). Previous studies have more focused on the horizontal water exchange rate in reservoirs, e.g., the exchange due to wind and anthropogenic regulation (Cai et al., 2018, Yang et al., 2022a), the exchange with the catchment (Ayala et al., 2014, Lewis et al., 2019), and the exchange in the confluences between mainstream and tributaries (Akiyama and Stefan 1984, Li et al., 2020b, Shi et al., 2022).

Vertical water renewal is usually complex, especially for impounded tributary bays, which possess both lacustrine and riverine characteristics. In such regions, vertical renewal can be controlled by several dynamic processes, such as thermal stratification, water circulation, river discharge and wind. Additionally, the difference in water density between the mainstream and the tributary generates remarkable intruding density currents that can affect both water and contaminant transport. Intrusion is the process by which the mainstream water enters the tributary at various depths matching the density. It is a unique hydrodynamic process in tributary bays of main reservoirs, and has been explored by means of observations (Ji et al., 2017, Yang et al., 2018) and modelling studies (Ma et al., 2015, Li et al., 2020a). All these processes interact and yield more complicated circulation patterns. Under such complex situations, it is difficult to evaluate the vertical renewal based solely on single hydrodynamic variables and thus, an auxiliary indicator is needed.

Water transport timescales are significant indicators for studying and predicting pollution hazards to the aquatic ecosystem. Therefore, transport timescales could be a quantitative approach for the vertical water exchange and further interpretation of the biogeochemical and biological processes (Xiong and Shen 2022). A variety of timescales have been introduced and utilized, including water age, residence time, flushing time, exposure time, and half-life time (Delhez et al., 1999, de Brye et al., 2012, Kwak and Cho 2019, Zhang et al., 2021). However, some timescales do not take the spatial-temporal heterogeneity into account and are difficult to evaluate in practice. For instance, bulk metrics like residence time, which is an integrative timescale, are less likely to capture the complex hydrodynamics at the resolution necessary to understand the biogeochemical processes (Gai et al., 2023). Among these timescales, water age is a helpful and practical approach for properly describing the spatial-temporal distribution of water renewal. The water age is defined as the time since it enters a specific domain, which can

be calculated by solving a set of partial differential equations based on the Eulerian theory (Deleersnijder et al., 2001, Delhez and Deleersnijder 2002, Gourgue et al., 2007). It has been applied extensively to investigate the flow and mass transport processes in both lentic (Bocaniov and Scavia 2018, Tang et al., 2021) and marine systems (Deleersnijder et al., 2001, Kärnä and Baptista 2016).

Traditionally, the quantifications of water age are mostly defined by flow times from upstream/downstream boundaries, seldom focusing on the vertical renewal originating at the surface. Though there are few oceanography studies applying the concept of vertical water age (*VWA*), i.e., the time since a water parcel last touched the water surface, to study the vertical transport of water in coastal oceans (Sun et al., 2019a, Xiong and Shen 2022), the timescale and the quantification of the water vertical renewal is still poorly understood in limnology. Moreover, the hydrodynamics in inland waters are very different from those in marine systems, especially in tributary bays affected by incorporating physical processes.

To address this, we employed the scaling approach - the *VWA*, and implemented it into a 3D hydrodynamic model (Delft3D-Flow), to study the vertical water renewal in Xiangxi Bay (XXB), a typical tributary bay of the TGR which has suffered water quality issues every year. A 3D hydrodynamics-based age model was established to provide a holistic understanding of the integrated effects of hydrodynamic processes, such as thermal stratification, intruding density currents from the mainstream, and upstream inflow, on the vertical water exchange. Although ultimately chemical evolution defines water quality, we explore the quantity of *VWA*, which has the advantage of being purely defined by physics and hence is perfectly suited to detect locations which are prone to deteriorate by limited exchange with the atmosphere. The main targets of this study are 1) quantifying the distribution and characteristics of vertical water renewal; 2) clarifying the effects of different hydrodynamic processes on vertical water transport; 3) investigating implications for water environmental issues and providing references for water environmental management. The findings provide new insights into quantifying vertical water transport in lakes and reservoirs with complex hydrodynamics and offer essential guidelines for environmental water management in highly dynamic systems using hydrodynamic indicators and approaches.

2 Materials and Methods

2.1 Study area

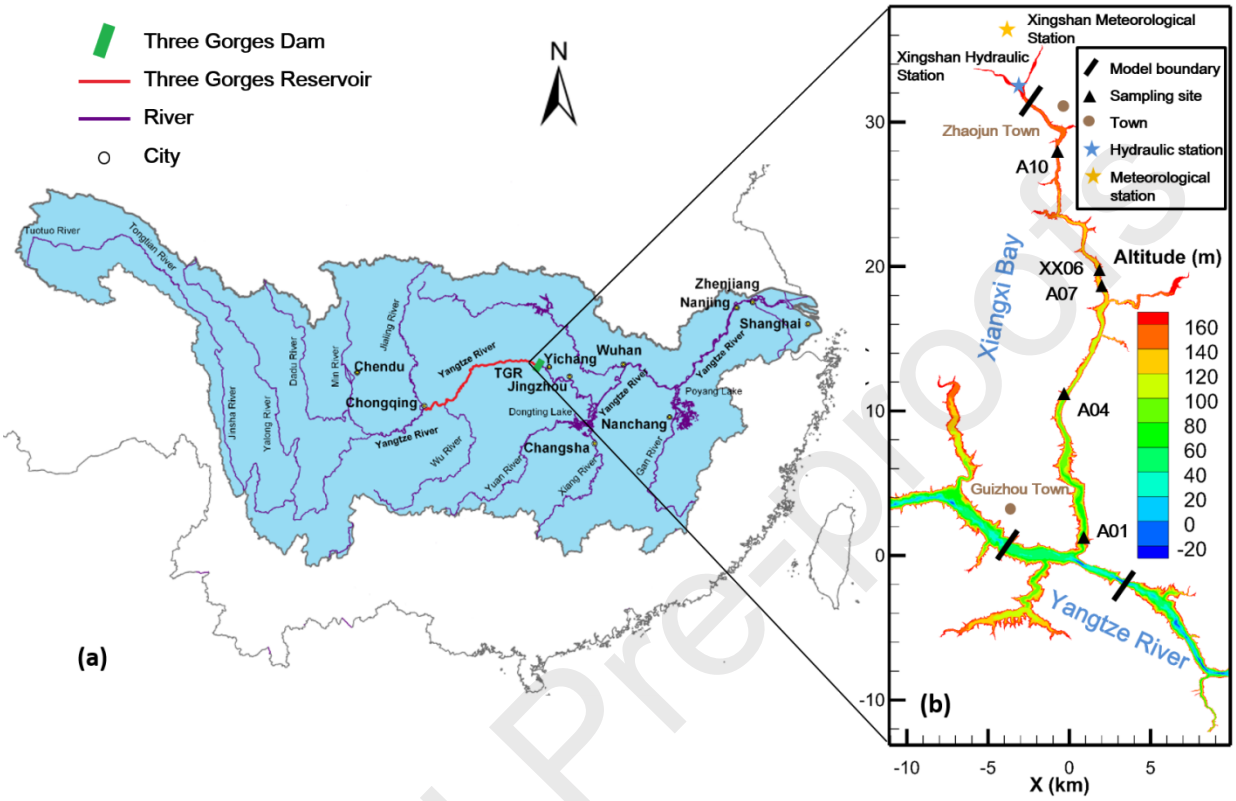

Figure 1. Geography of the TGR and XXB. (a) The Yangtze basin, with the locations of the Three Gorges Dam and TGR. (b) The study area of model, with elevation of the XXB bottom, locations of the model boundaries, gauge stations, and sampling sites in the XXB.

The TGR is one of the largest artificial reservoirs in the world (Figure 1a). This riverine reservoir is very long (667 km) with a maximum depth of ~150 m when the water level reaches 175 m above sea level at the end of autumn and winter. It has a total surface area of about 1084 km^2 and total storage capacity of 39.3×10^9 m^3. The TGR is located in a subtropical climate, with an average air temperature of 17.6 °C and an average monthly water temperature above 10 °C. The TGR operation cycle is divided into four stages according to water level and discharge: normal operation (November to January), drawdown (February to early June), low water level operation (June to August) and impoundment (September to October).

Xiangxi River is one of the largest tributaries of the TGR and, at a distance of 32 km, is the nearest tributary to the dam wall. The mainstream of the Xiangxi River is about 94 km long, the catchment basin area is 3099 km^2, the average annual flow is 47.3 m^3 s^{-1}, and the maximum

discharge can reach 300 m^3 s^{-1}. The average monthly retention time in XXB ranges from 7 to 16 days (Liu et al., 2013). Before the impoundment of the TGR in 2003, the flow velocity in the Xiangxi River was very fast due to its large bed slope (2.7‰). No phytoplankton blooms of concern had been reported. The impoundment of the TGR significantly increased the water level, greatly reduced the flow velocity in the Xiangxi River, and formed a side arm of TGR called Xiangxi Bay. Seasonal stratification, especially strong summer stratification, occurred in XXB, whereas the mainstream of the TGR is seldom affected by seasonal stratification due to the large runoff and strong mixing.

The research area included 32 km of the river reach of the Xiangxi River from the upper reaches of Zhaojun Town to the intersection of the Xiangxi and Yangtze Rivers, and a 7 km reach of the Yangtze River at the intersection to the XXB (Figure 1b). The maximum depth in the study area of XXB reached ~100m. Water temperature and flow velocity were measured at observation points A01, A04, A07, A10, and XX06 in the XXB. Water temperature profiles were measured with a Hydrolab DS 5X multi-probe sonde (Hach, USA), at a vertical resolution of 1 m. Velocity profiles were measured with an Acoustic Doppler Vectir velocimeter (ADV; Nortek, Norway) at depths of 0.5 and 2 m and then to the bottom at 2 m intervals. Measured temperature and velocity profiles on August 02 were collected from Gao et al., (2018).

2.2 Model description

1) Hydrodynamic model

The TGR impoundment increased the water surface width in the lower reach of the XXB to 300 - 600 m. Nevertheless, compared to the horizontal direction, the vertical water flow was comparatively weak. For such a condition, the shallow water equations with the Boussinesq approximation were appropriate for characterizing the water movement in the XXB. In this study, the 3D model Delft3D-Flow (Deltares 2013) was applied to simulate the hydrodynamics in XXB. An orthogonal curvilinear grid was used in the horizontal direction and z-coordinate was used in the vertical direction due to the steep topography of the XXB in our study. In this case, the z-coordinate system is more suitable than the σ-coordinate system to calculate the vertical exchange processes due to the existence of vertical stratification. The model solves shallow water equations (with the hydrostatic and Boussinesq hypothesis) derived from the Reynolds-averaged Navier-Stokes equations for an incompressible fluid, and four different turbulence closures are implemented to determine the vertical eddy diffusion caused by turbulent mixing. The Delft3D-Flow model is designed to effectively solve the shallow water equations in the horizontal direction by using the Alternative Direction Implicitly (ADI) approach (2D). The vertical velocity is calculated by integrating the mass conservation equations and the horizontal velocities averaged over the water depth.

2) Water age model

The current research focuses on the departure of water from the water surface of the XXB. The *VWA* represents the timescale of vertical transit of water in the bay beginning when a water parcel leaves the surface. The trajectory of a water parcel is illustrated in the Lagrangian description (Figure 2). When a water parcel is located at the surface, i.e. at A or E in Figure 2, its age is set to zero. When the parcel leaves the surface, its age begins to increase (e.g. from B to D). Because the riverbed is assumed to be impermeable, the age continues to increase even if the parcel touches the riverbed (from C to D). The parcel's age is reset to zero when it returns to the surface and the age clock starts again when it re-enters the water body. It should be noted that a water parcel does not always touch the riverbed, i.e., point C is not always at the riverbed, and the age value may still be calculated in such circumstances.

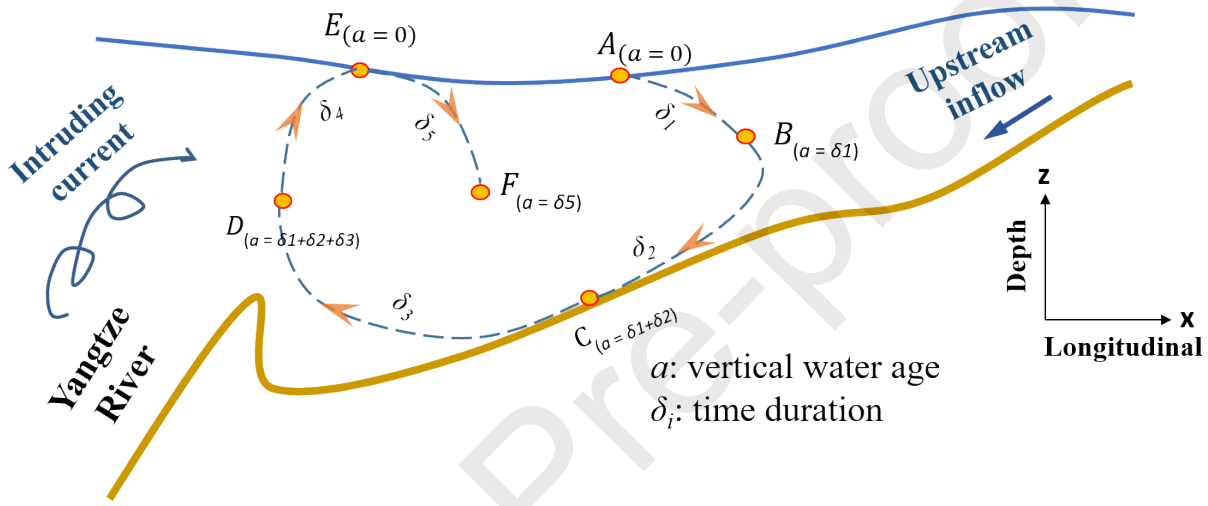

Figure 2. Schematic diagram of *VWA* for vertical water renewal, whereby the age of a water parcel grows until re-touching the surface. (Note x is the direction along the thalweg of the Xiangxi River, and z is the direction along the depth.)

In the Eulerian approach, the general kinetic process of age can be described by two partial differential equations and one algebraic equation (Delhez and Deleersnijder 2002), as expressed by Eqs. 1a, 1b and 1c:

$$\frac{\partial C}{\partial t}+(\nabla_{\mathrm{h}}\cdot\vec{u})C+\frac{\partial wC}{\partial z}=\nabla_{\mathrm{h}}\cdot(D_{\mathrm{h}}\nabla_{\mathrm{h}})C+\frac{\partial}{\partial z}(D_{\mathrm{v}}\frac{\partial C}{\partial z}) \qquad (1a)$$

$$\frac{\partial \alpha}{\partial t}+(\nabla_{\mathrm{h}}\cdot\vec{u})\alpha+\frac{\partial w\alpha}{\partial z}=\nabla_{\mathrm{h}}\cdot(D_{\mathrm{h}}\nabla_{\mathrm{h}})\alpha+\frac{\partial}{\partial z}(D_{\mathrm{v}}\frac{\partial \alpha}{\partial z})+C \qquad (1b)$$

$$a=\frac{\alpha}{C} \qquad (1c)$$

where a is the water age; α is the age concentration; C is the tracer concentration referring to the proportion of traced water that has touched the water surface. It stands for the aging process: α grows by C every time step; $\vec{u} = (u, v)$ and w are the horizontal and vertical velocity components, respectively; D_h and D_v are the horizontal and vertical diffusivities, respectively; $\nabla_h = (\partial/\partial x, \partial/\partial y)$ is the horizontal vector differential operator (h-Del operator).

The age model was built by modifying the source codes of the conventional advection-diffusion module in the Delft3D-FLOW model according to Eqs. 1a and 1b. To track water age, we added three constituents, which represented C, α, and a, respectively, in the 'Pollutants and tracers' of 'Processes' module in the Delft3D GUI. The water age evolution was driven by the basic hydrodynamic parameters derived from the hydrodynamic model, such as water level, velocity, and diffusivity. The age model was then integrated with the hydrodynamic model to mimic the kinetic process of water age. In contrast to the traditional concept of water age, which uses the upstream/downstream boundary for the water age calculation, we set the water surface as the boundary condition by assigning values to surface concentrations of C and α in the whole domain for every time step by modifying the source codes. Specifically, at the surface boundary, the tracer concentration is set to one, and the age concentration is set to zero, i.e., $C = 1$, and $\alpha = 0$. For the rest of the domain, initially, both tracer concentration C, and age concentration α are set to zero.

2.3 Model setup and data

The model area included the XXB and a part of the Yangtze River. The XXB comprised 407 longitudinal and 16 lateral grid cells, each with a grid size of ~100 m × 40 m (longitudinal × lateral). The Yangtze River contained 69 longitudinal grids and 20 lateral grids with a grid size of ~150 m×70 m (longitudinal × lateral). As the use of the σ-coordinate system could result in numerical inaccuracies to the positions of density iso-surfaces due to the quite steep bed slope in the research area (the slope exceeds 0.5 in the lateral direction) (Ezer and Mellor 2004), the z coordinate system was used in this study. In the vertical direction, we used a total of 100 layers, with the 80 upper layers each having a thickness of 1.5 m, and the 20 lower layers each having a thickness of 4.0 m. The maximum depth of XXB was ~100 m, which meant the calculation in the XXB was only based on the upper 80 layers as the deepest location of XXB lay higher than the mainstream bed of the Yangtze River. Therefore, vertical processes like density currents could be well mimicked in the XXB since the upper layers covered all the depth inside the bay. On the other hand, the bottom 20 layers were set for calculating the mainstream, which had a lower elevation and was mostly mixed all the year round.

The model had two upstream boundaries and one downstream boundary (Figure 1b). The XXB upstream boundary is located close to Zhaojun Town, and the upstream boundary of the Yangtze River is located near Guizhou Town. The downstream boundary of the Yangtze River was set 4 km downstream from the intersection area of the XXB and, was set as an open

boundary. The inputs for the upstream boundary were river inflow and inflow temperature. The inputs for the downstream boundary were water level and water temperature. The daily average river inflow and inflow temperature for the upstream boundary of the XXB were obtained from the Xingshan Hydrological Station (Figure 1b). The daily average river inflow, inflow temperature and water level data at the upstream/downstream boundary of the Yangtze River were derived from a 1D longitudinal hydrodynamic model (Sun et al., 2019b) since the hydrological stations on the mainstream were far away from the boundary set by our model. This was considered to be reasonable because the boundaries at the Yangtze River located in the mainstream where the water temperature was mostly well-mixed in the lateral and vertical direction. We used the daily data obtained from the China Meteorological data at the Xingshan meteorological observation station, including air temperature, wind speed and wind direction for the meteorological input (Figure S1). The tracer concentration, C, and the age concentration, α, were set to zero for the upstream and downstream boundaries, to avoid counting the time since the water parcel left the upstream/downstream boundaries (see more details in Text S3 and Figure S3). The model simulation ran from September 01, 2009 to December 31, 2010, with a cold start (the velocity was set to zero, the temperature was set to the arithmetic mean of values of the upstream boundaries as the Yangtze mainstream was mostly well-mixed in both lateral and vertical direction), the four-months simulation of 2009 was for spin-up and the 2010 results were used for analysis. The time step was set to 0.6 min.

The shorelines change as a result of the shifting water levels. Thus, a flooding and drying algorithm was used to locate the model boundary to account for this and ensure the conservation of mass and momentum. The "excess temperature" option in Delft3D-Flow was used to compute the heat flux between the air and water surface, which was implemented as a function of the temperature difference between the air and water surface (Deltares 2013). The equation proposed by Qin (1980) was used to compute the wind stress at the water surface. The k-ε turbulence closure was selected to compute the vertical turbulent eddy viscosity and turbulent diffusivity. More details are given in Deltares (2013).

The water temperature and flow velocity were calibrated against measured data. Specifically, we calibrated the horizontal eddy viscosity coefficient, horizontal diffusion coefficient, and bottom friction coefficient (Manning coefficient) manually by minimizing the root mean square error (*RMSE*). These parameters are the main and common parameters to be calibrated for Delft3D-Flow model (Mao et al., 2015, Goede 2020, Song et al., 2021a). After a manual "trial and error" procedure, the simulation results and the measured results showed good agreement when these parameters were set to 1.0 $m^2 s^{-1}$, 0.2 $m^2 s^{-1}$, and 0.01 $s \cdot m^{1/3}$, respectively (see details of the calibrated parameters in Table S1). Statistical indices, such as the mean absolute error (*MAE*) and the *RMSE* were used to quantitatively assess the quality of fit and errors between the observed and simulated data.

The surface and bottom layers are defined as the surface cell and the cell immediately above the bottom of our model, respectively (Bocaniov et al., 2020). The determination of the mixed layer depth (surface mixed layer; MLD) followed a method commonly employed in related studies conducted at the same research site (Xu et al., 2021, Yang et al., 2022b), which involved identifying the depth at which the temperature deviated by 0.5 ºC from the surface temperature, as per the approach detailed by de Boyer Montégut (2004). This approach was insensitive to variations in the vertical resolution of water temperature data. Additionally, the temporal pattern in response to alterations in the threshold value (Wilson et al., 2020), particularly when considering the complex hydrodynamics in XXB. Stratification was inferred when the temperature gradients exceeded 0.05 °C m^{-1}, and weak stratification was inferred when temperature gradients were around 0.05 °C m^{-1}. This definition was more appropriate for lentic systems with fluvial intrusions (McCullough et al., 2007).

2.4 Model validation

The hydrodynamic performance was verified against the measured water temperature and flow velocity profiles (Figure 3 and Figure 4). The modelled water temperature agreed well with the field data, with the *MAE* and *RMSE* values mostly less than 1.0 °C at four sites (XX06, A10, A04, and A01) on different dates (nine dates at XX06, three dates at both A10 and A04, and one date at A01) (Figure 3). There were discrepancies in the surface simulation results at station XX06 on July 02 and August 02, and at station A10 on August 02. These discrepancies might be caused by the spatial inhomogeneity of meteorological data, which we did not account for but might influence the surface water temperature. However, the model could still have captured the thermal structures satisfactorily despite the surface deviations.

The flow velocity was verified with the data at three sites (A10, A07, and A04) on three dates (April 28, August 02, and October 10) (Figure 4). The modelled flow velocity was in good agreement with the measured data. The *MAE* was between 0.014 m s^{-1} and 0.039 m s^{-1}, and the *RMSE* was between 0.017 m s^{-1} and 0.042 m s^{-1}. The poorer results mainly occurred at station A10 (Figure 4a), and were likely due to some inaccuracies in the upstream inflow input. Additionally, there were discrepancies in the bottom layers of A04, which might be caused by low resolution of the bottom layers (Liu et al., 2014). It might also be because the flow velocity was measured instantaneously, whereas the hydrological and meteorological data used in the model were daily averages, so the model might not capture such instantaneous variations in flow velocity.

The model performance of simulating hydrodynamic processes was satisfactory compared to those reported in previous studies (Ma et al., 2015, Gao et al., 2018, Chuo et al., 2019, Song et al., 2021b, Chen et al., 2022), which confirmed that the model could capture the advection-diffusion process and establish a good foundation for the *VWA* simulation.

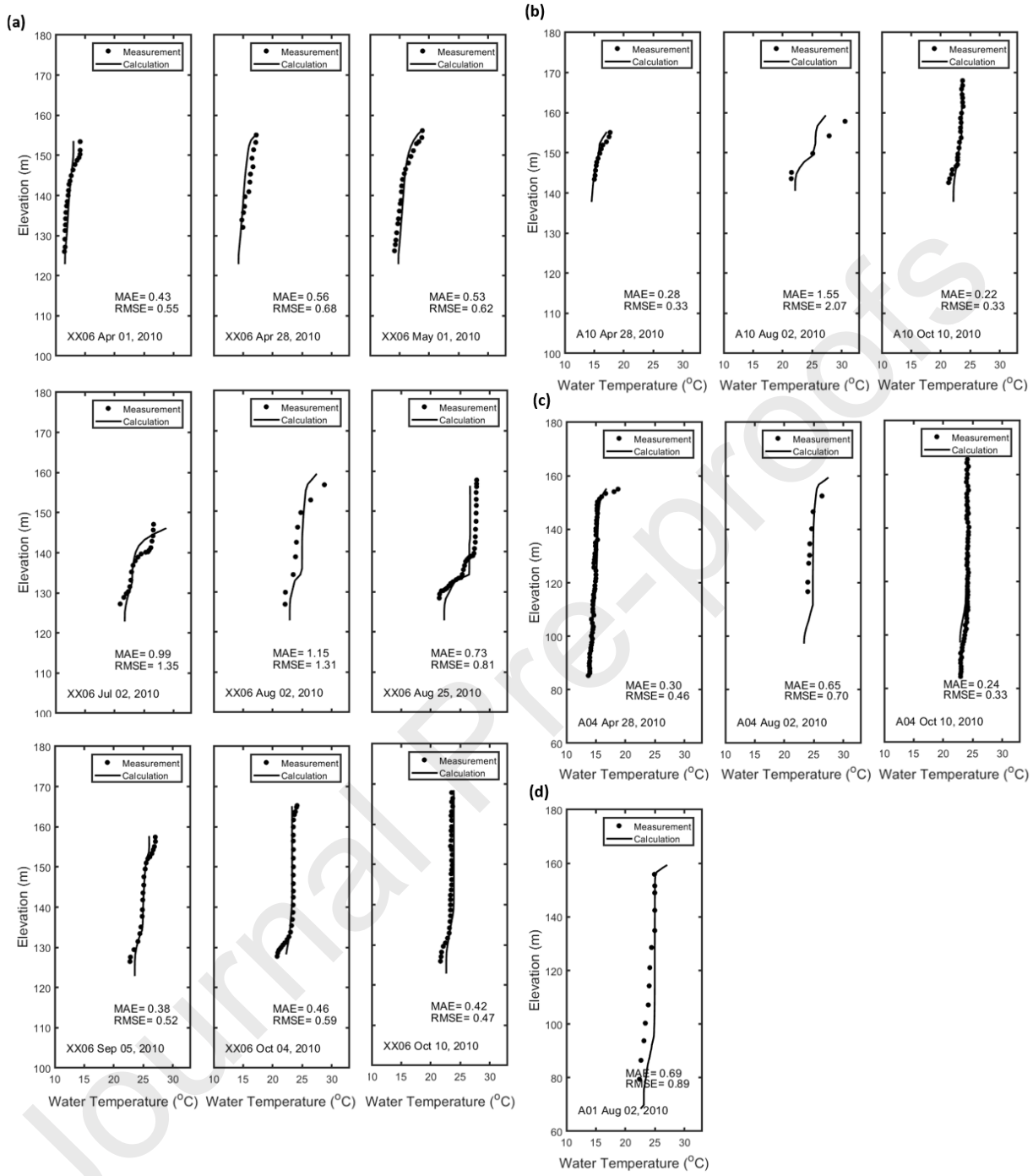

Figure 3. Comparisons of measured (solid symbols) and simulated (black lines) water temperature at (a) station XX06 in the middle reaches on April 01, April 28, May 01, July 02, August 02, August 25, September 05, October 04 and October 10, respectively, (b) station A10 at the upper reaches on April 28, August 02, and October 10, respectively, (c) station A04 at the lower reaches on April 28, August 02, and October 10, respectively, and (d) station A01 at the lower reaches on August 02.

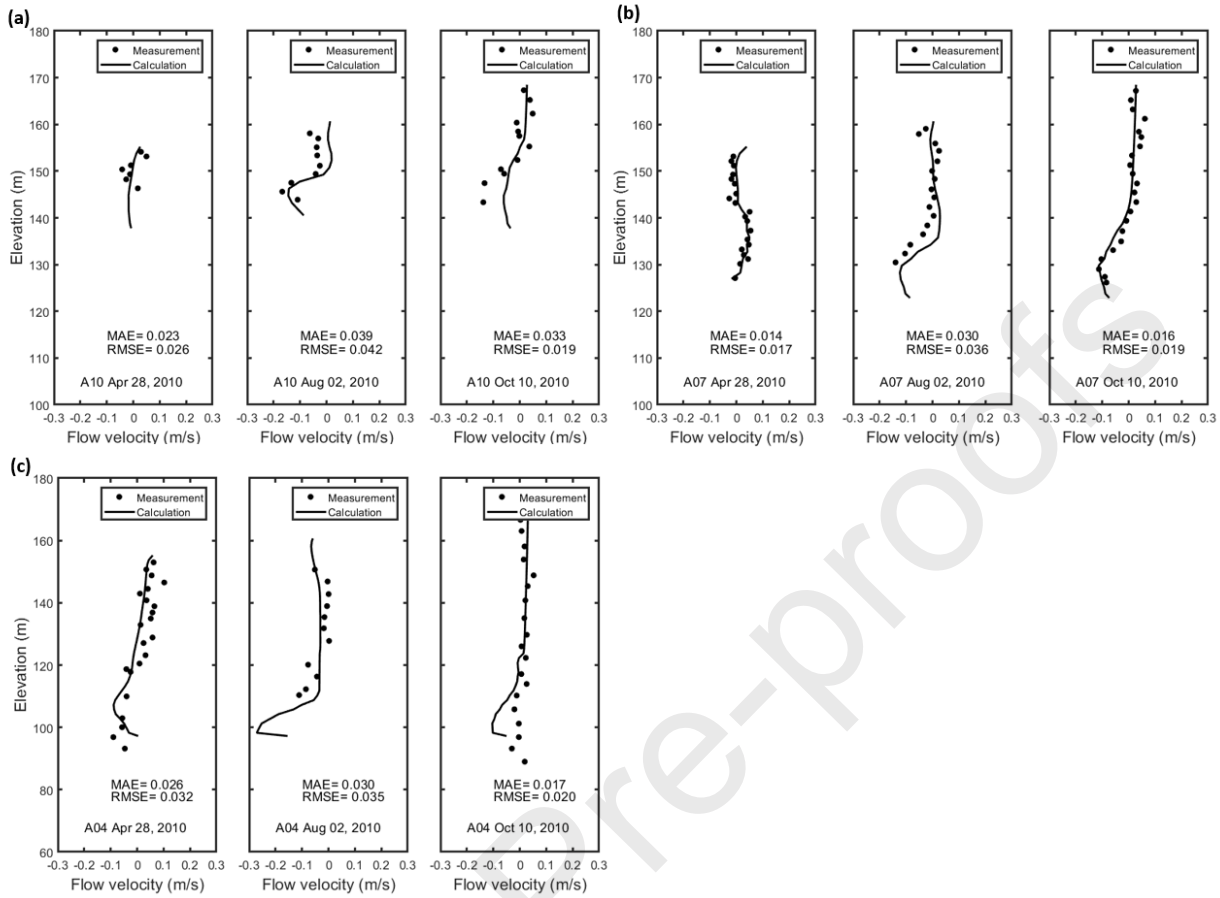

Figure 4. Comparisons of measured (solid symbols) and simulated (black lines) flow velocity at (a) station A10, (b) station A07, and (c) station A04, on April 28, August 02, and October 10, respectively.

3 Results

3.1 Water temperature and density currents distribution

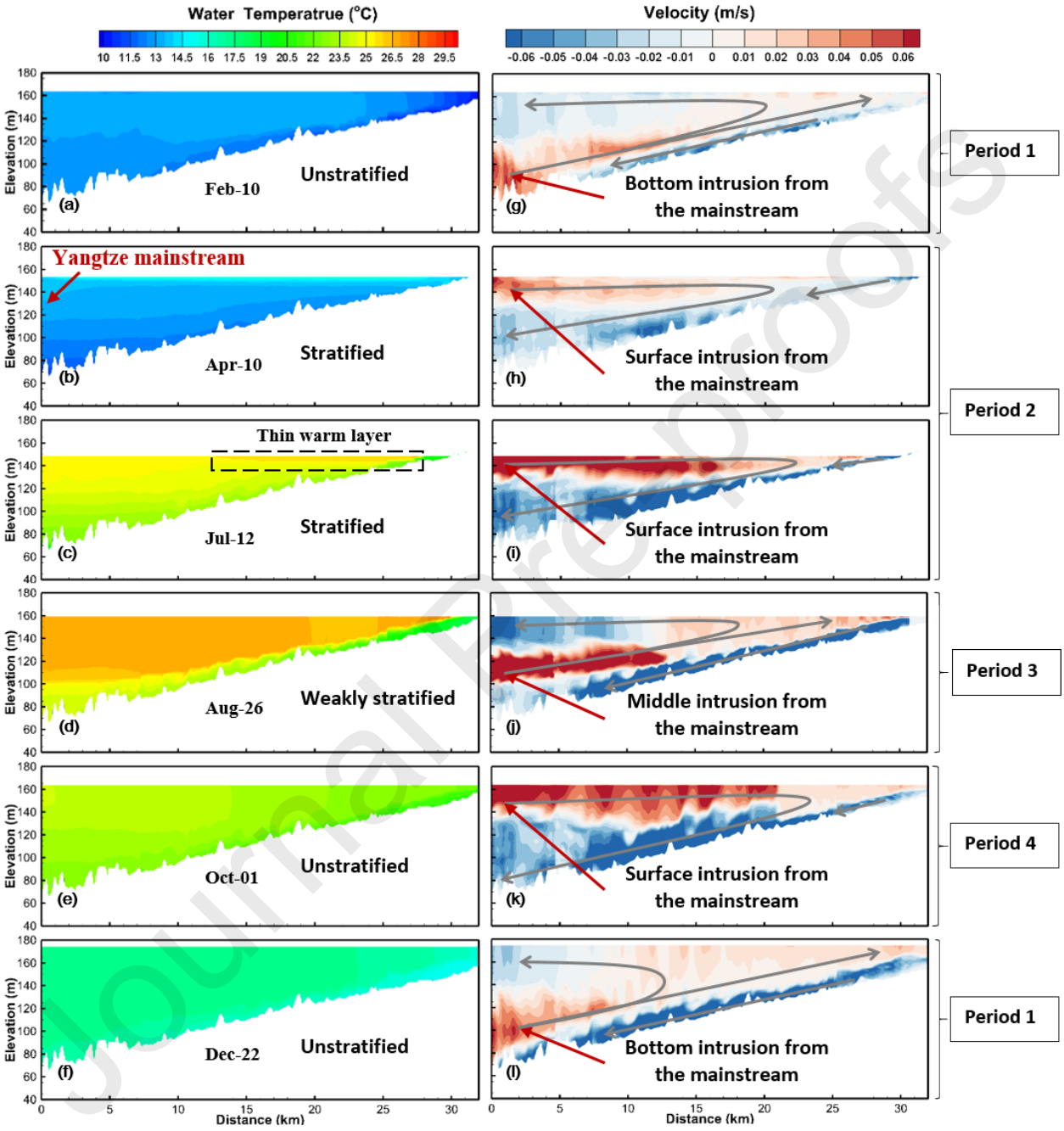

Figure 5. Water temperature (left side) and longitudinal flow velocity (right side) distribution along the thalweg in XXB at different times in 2010. Currents towards the upstream inflow are represented by warm colours, while currents towards the mainstream are shown in cool colours, respectively. The circulation patterns are represented by grey arrows. (left side of each plot indicates the intersection of Yangtze mainstream and Xiangxi River.)

Due to different densities produced by temperature differences between the mainstream and tributary, density currents from the mainstream intruded into the XXB from the surface, middle, and bottom layers at various times (shown in Figure 5g-l, hereafter surface intrusion, middle intrusion, and bottom intrusion). Hence, we divided the year 2010 into four periods according to the regular stratification patterns and different forms of intruding density currents from the mainstream. **Period 1** (Figure 5a and g, f and l): from the end of October to mid-March, the intruding currents entered XXB from TGR in the bottom layers. The upstream-flowing currents floated up to the upper layers and flowed back downstream at the surface, forming an anti-clockwise circulation in our depiction. The temperature difference between the surface and bottom layers was 0.5-1 °C, and there was almost no stratification; **Period 2** (Figure 5b and h, c and i): from mid-March to the end of August, the intruding water mostly entered at the surface, moved upstream and then flowed back downstream in the bottom layers, generating a clockwise circulation. The water temperature difference reached 2-6 °C, and a significant stratification appeared in the entire bay; **Period 3** (Figure 5d and j): from the end of August to the end of September, the intruding water entered at mid height, the water temperature difference was 1.5-4 °C, and the stratification disappeared gradually. The water was well mixed both in the surface and middle layers, and there was only stratification in the bottom layers between the intruding water and upstream inflow; **Period 4** (Figure 5e and k): from the end of September to the end of October, the intruding water entered into the surface layers, the water temperature difference was about 1 °C, and there was almost no stratification in most of the bay.

3.2 Special thermal structures

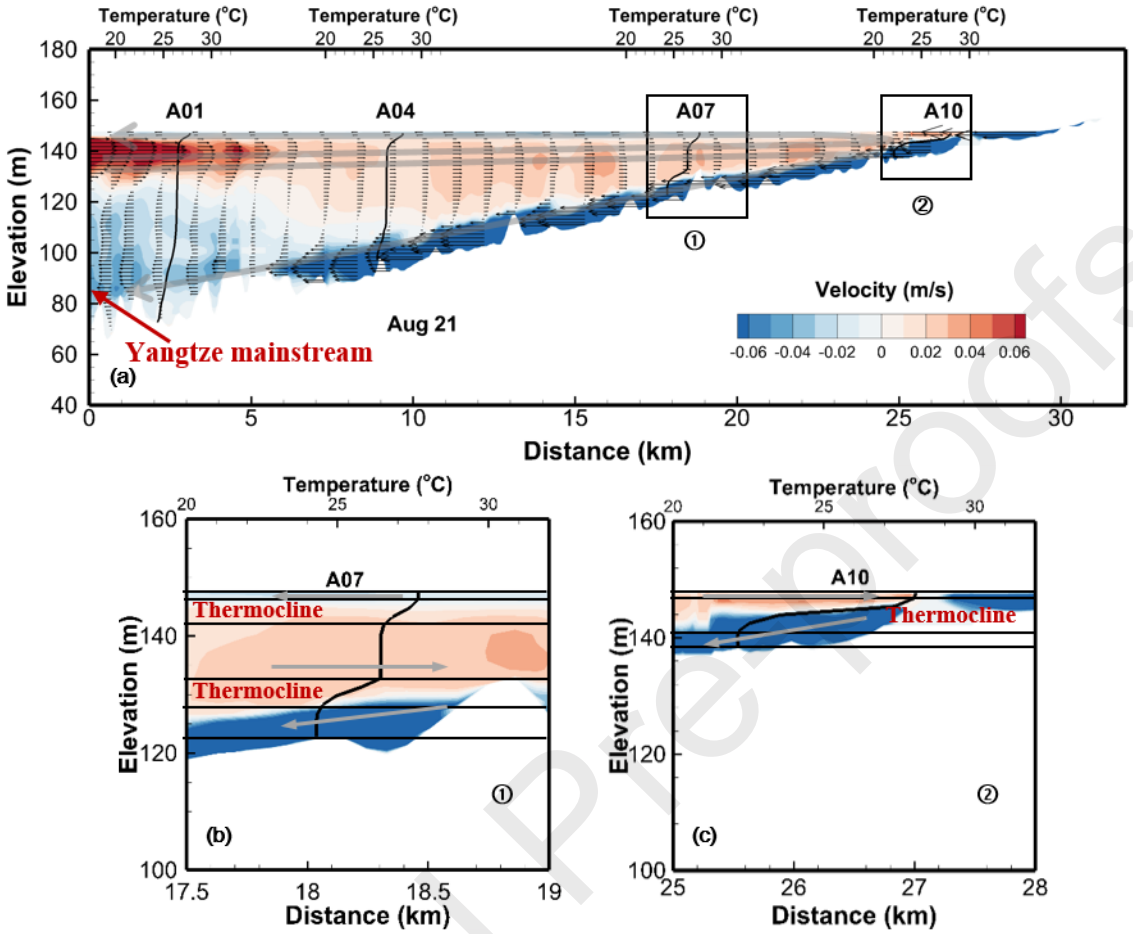

Figure 6. Temperature profiles (black lines) and velocity distribution (colour contours) on Aug. 21st. The intrusive (upstream-flowing) and downstream-flowing currents are represented by warm and cool colours, respectively.

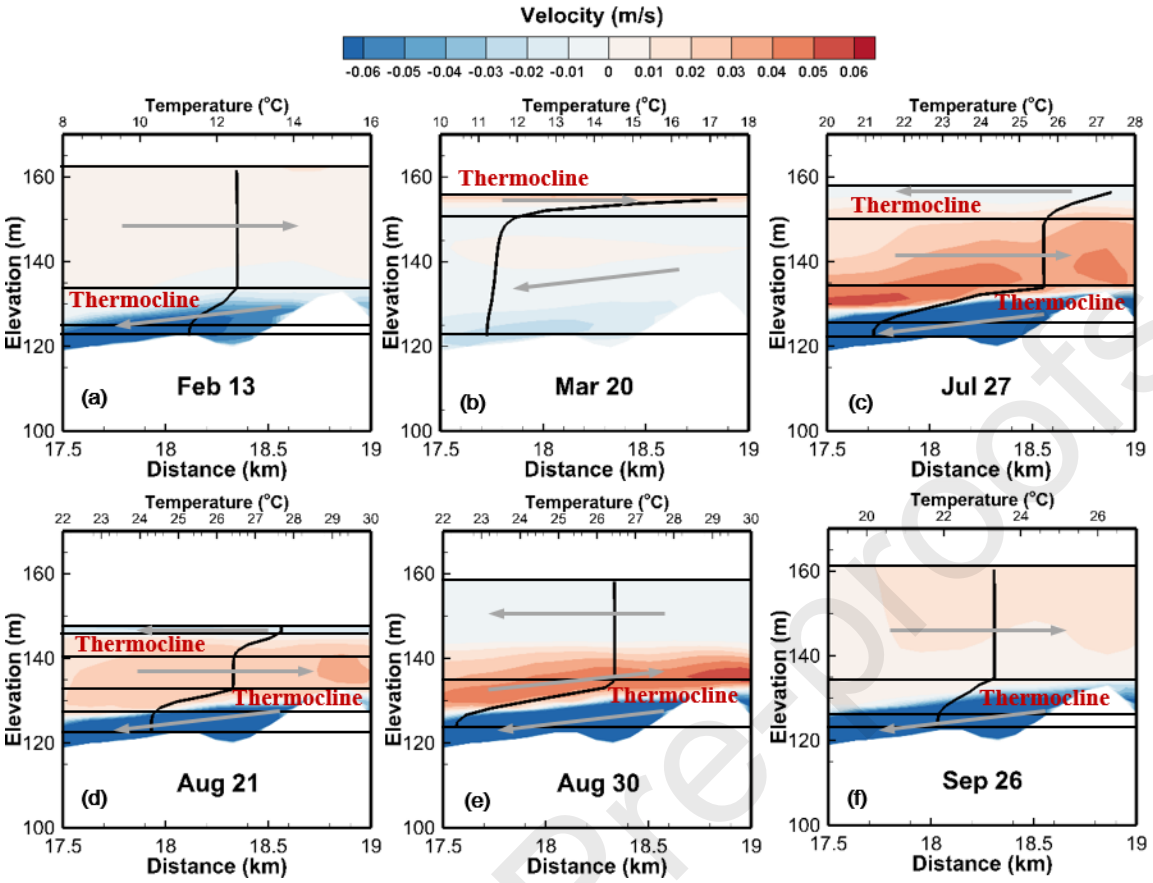

Figure 7. Temperature profile (black lines) and velocity distribution at the middle reach (A07) on various days in 2010. The intrusive (upstream-flowing) and downstream-flowing currents are represented by warm and cool colours, respectively. The arrows indicate the flow direction.

Thermal structures in XXB displayed unique characteristics under the integrated effects of intruding density currents, stratification and upstream inflow (Figure 6 and Figure 7). For instance, at the end of August, the density currents from the mainstream intruded at the subsurface, tracing upstream from this layer. The compensation flow returned to the estuary from the surface and bottom layers, respectively, forming two large circulations (Figure 6a). Under the effect of this complex circulation, often four or even five-layered stratification patterns formed, and were different from the typical three-layered patterns in natural lakes. The lower reaches (Station A01, A04) showed a three-layered stratification, and the thermocline appeared at the interface between the intruding current (shown as warm colour) and surface compensation inflow (shown as cold colour). The waterbody below the thermocline was mixed with no obvious temperature gradient under the combined effect of intruding currents and upstream underflow. The middle reaches (Station A07) showed a special five-layered stratification pattern (Figure 6b). The surface water was mixed under the effect of wind and surface compensation flow, the bottom and middle water were respectively mixed by the underflow from upstream and the intruding water from the mainstream. At the interface between the intruding currents and surface compensation flow, and between the intruding currents and the upstream underflow at the bottom

layer, respectively, two thermoclines formed. In the upper reaches (Station A10), three-layer stratification emerged again. However, during this time, the thermocline appeared at the interface between the intruding current and upstream underflow.

In the middle reaches, the intruding currents and the upstream inflow converged, and special thermal structures formed throughout the whole year. In **period 1** (Figure 7a), a three-layered pattern formed, and the temperature difference between the surface and the bottom was about 1 °C. The surface and bottom waters were well-mixed, and a thermocline formed at the interface between the intruding currents at the surface and the upstream underflow at the bottom layer. In **period 2** (Figure 7b), the water column presented a two-layered stratification pattern at the beginning, and the temperature difference between the surface and the bottom was about 6 °C. A large temperature gradient of about 1 °C m^{-1} formed at the surface layer. Then, in summer, the water column presented a four-layered stratification pattern, and the temperature difference was still about 6 °C (Figure 7c). Two thermoclines formed, one was between the surface compensation flow and the middle intruding water, and the other one was between the middle intruding water and the upstream underflow at the bottom. During some special periods (Figure 7d), as the air temperature rose rapidly, the very surface layer was heated evenly and well mixed, and a unique five-layered stratification pattern formed. The temperature difference was about 3.5 °C. In **period 3** (Figure 7e), only in the middle layers, a thermocline formed between the intruding water and the upstream underflow. The water column formed a two-layered pattern, with a temperature difference of about 3.5 °C. In **period 4** (Figure 7f), similar to that in period 1, the water column was stratified into three layers, and the water temperature difference was about 1 °C.

3.3 Vertical water age distribution

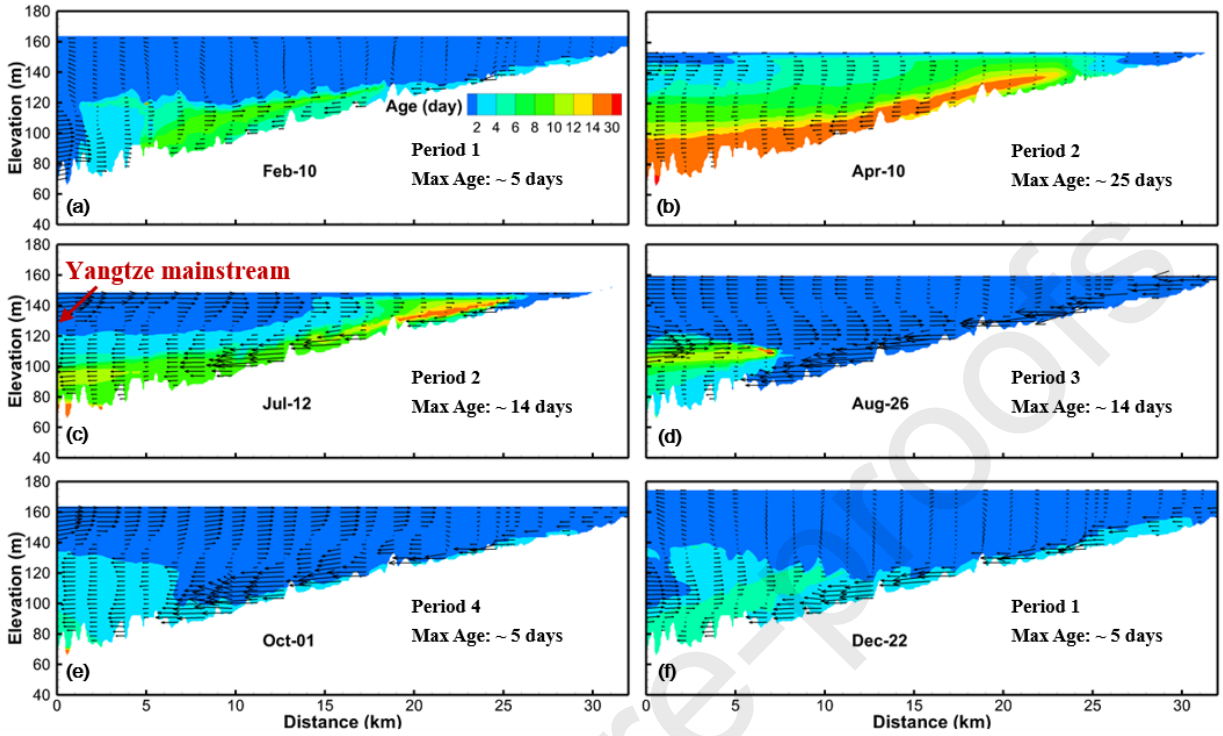

Figure 8. *VWA* distribution along the thalweg at different times of the year. The arrows represent the currents. Note that left sides of each plot indicate the intersection of Yangtze mainstream and Xiangxi River.

In **period 1** (Figure 8a and f), the vertical water exchange was fast at the upper and middle layers and the *VWA* was small. The maximum age was ~5 days, appearing at the bottom of the middle and lower reaches. In **period 2** (Figure 8b), *VWA* was larger, reaching ~30 days at the bottom of the lower reaches. In summer (Figure 8c), the *VWA* remained large, with the maximum value of about 20 days in the middle layer of the upper and middle reaches. In **period 3** (Figure 8d), the *VWA* decreased significantly, the maximum value decreased to ~10 days in the middle layers of the lower reaches. The middle intrusion currents broke the stable stratification patterns in the middle and bottom layers and accelerated the vertical water renewal. The larger upstream inflow also brought the bottom trapped water to the mainstream and, hence, reduced the *VWA*. In **period 4** (Figure 8e), the *VWA* was very small, the maximum value was only ~5 days, appearing at the bottom of the lower reaches. During this time, intense mixing greatly accelerated the vertical water renewal. Combined with the effect of circulation, the vertical water exchange was fast in the entire bay.

The monthly medians of age were less than 10 days (Figure 9), and showed a clear seasonal trend: large in the spring and summer, and small in the autumn and winter. The

maximum *VWA* was ~25 days, appearing in April. The maximum value in spring and summer was over 15 days except for June. During spring and summer, age dropped to a low value in June, which was due to the significant increase in upstream inflows at that time (Figure S1d). In addition, the deviation of *VWA* in spring and summer was larger, indicating a larger spatial (both vertical and horizontal) inhomogeneity.

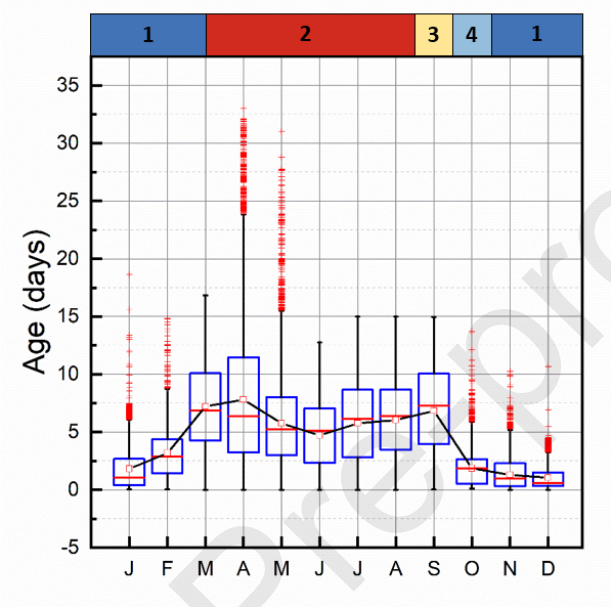

Figure 9. *VWA* of the whole bay. Red lines denote medians of *VWA*, empty red squares joined by lines denote the mean *VWA*, blue rectangles denote the first and third quartiles, the whiskers represent the maximum and minimum value, and red crosses denote the outliers. The numbers on the label show the period that we divided.

3.4 Impact of stratification on vertical water exchange

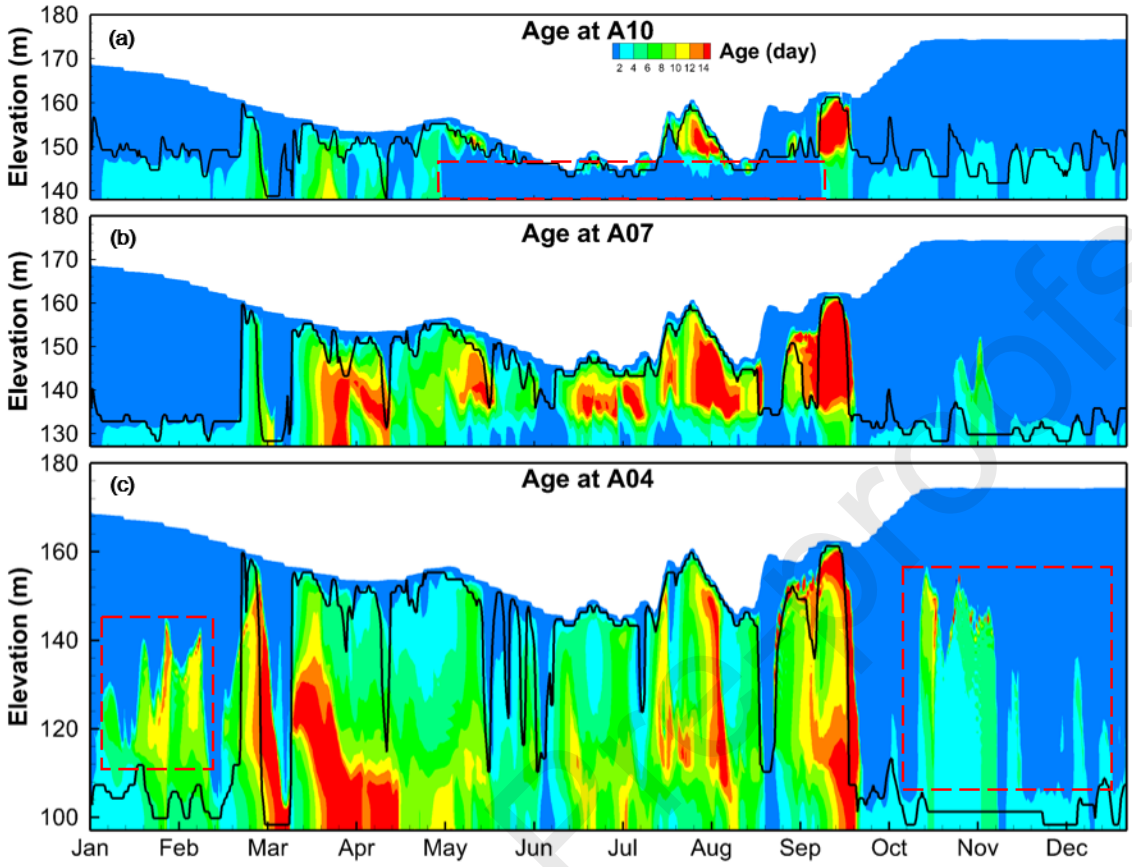

Figure 10. *VWA* distribution and mixed depth layer (black lines) in the (a) upper (A10), (b) middle (A07) and (c) lower (A04) reaches, respectively.

In the mixed surface layer, the *VWA* was usually very small (less than 2 days). The waterbody was thoroughly mixed and the water exchange was fast. Along depth, the *VWA* increased significantly below the mixed layer because the thermocline inhibited the vertical exchange. However at the upper reaches (Figure 10a), the *VWA* below the MLD was very small (less than 2 days) from May to September (shown by the red dotted box), which was much smaller than the middle layers of the middle reaches. This might be attributable to the flushing from the upstream inflow. This period was in the flood season, with high upstream inflow (Figure S1c), which flowed along the riverbed to the confluence area and accelerated the renewal of the underlying trapped water, and consequently decreased the *VWA*. On the other hand, at the lower reaches (Figure 10c), during the winter from January to February and from October to December, there was still a high *VWA* above the mixed layer (the maximum age value was about 12 days in the middle layers) which might have originated from trapping water parcels inside the circulation.

The relationship between the MLD and *VWA* shared a similar pattern at the upper, middle, and lower reaches, but exhibited both spatial and temporal variations (Figure 11). In the middle reaches where the vertical renewal was mainly affected by turbulent mixing, the distribution of points varied considerably between periods (Figure 11b): In **period 1**, the *VWA* varied inversely with the MLD. The MLD was mostly greater than 20 m and the *VWA* decreased rapidly (blue points in the blue ellipse). In contrast in **period 2,** the *VWA* did not change noticeably with the MLD. The MLD was between 1-10 m and the *VWA* was larger, about 10 days (red points in the red ellipse). However, the data points of **period 3** and **4** were distributed in both ellipses (yellow and light blue clusters) which were likely because they were in the transition period.

In the upper reaches (Figure 11c), which were heavily influenced by the upstream flushing, the data in different periods were more scattered, with a much higher variance than in the other locations. Nevertheless, a certain inverse relationship still existed. This suggested that vertical renewal was hindered where the water was stratified.

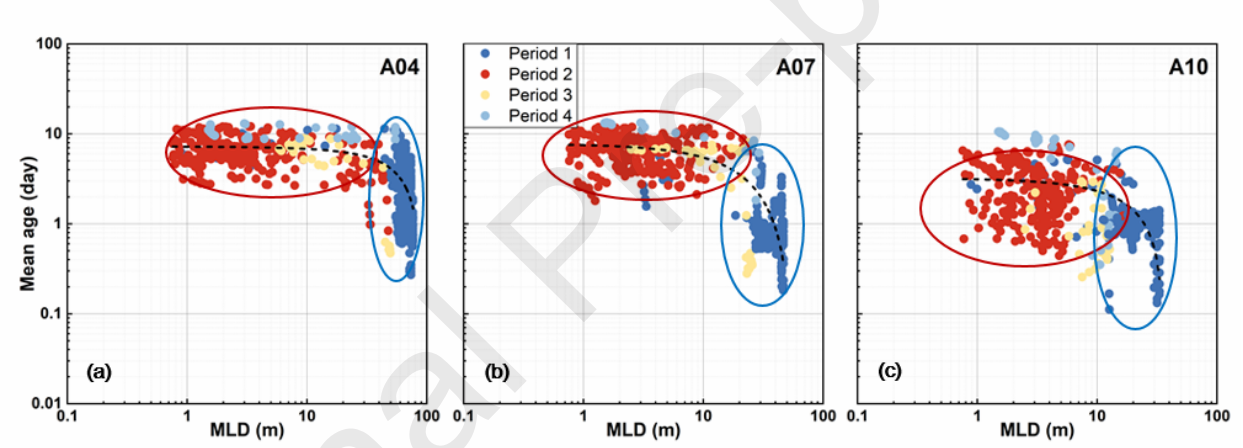

Figure 11. Mean *VWA* versus MLD in the (a) lower (A4), (b) middle (A07) and (c) upper (A10) reaches, respectively. Dots are coloured according to the periods we defined.

3.5 Impact of intruding currents on vertical water exchange

During the bottom intrusion period, the *VWA* was markedly smaller than during the middle and surface intrusion periods (Figure 12). The bottom intrusion broke the stable thermal stratification and the resulting circulation accelerated the removal of the trapped bottom water. In contrast, when the intrusion occurred at the surface, stable thermal stratification formed easily. At this time, the *VWA* was large in the middle and lower reaches (Figure 12a and b), with a maximum bottom age of ~20 days in the lower reaches. The middle intrusion period was in the transitional period from the surface intrusion to the bottom intrusion. In this period, the *VWA* was also relatively large, especially in the middle reaches of the XXB, and the age was significantly larger than in other periods (Figure 12b).

In terms of spatial distribution, in the middle and lower reaches, which were mostly affected by the intruding density currents, *VWA* varied significantly with the circulation pattern, and the maximum bottom age could differ by ~15 days in the lower reaches (surface intrusion period was ~60% larger than the bottom intrusion as shown in Figure 12a). In the upper reaches (Figure 12c), which were less affected by the density currents, *VWA* variations were not sensitive to these three modes of intrusion.

In addition, the bottom water was younger than the depth-averaged age when there was surface and middle intrusion, but not bottom intrusion (Figure 12). Especially during periods of middle intrusion, the depth-averaged age was ~50% larger than bottom age (the median bottom age was 5 days, 3 days, and 2 days, while the median depth-averaged age was 8 days, 7 days, and 4 days, respectively).

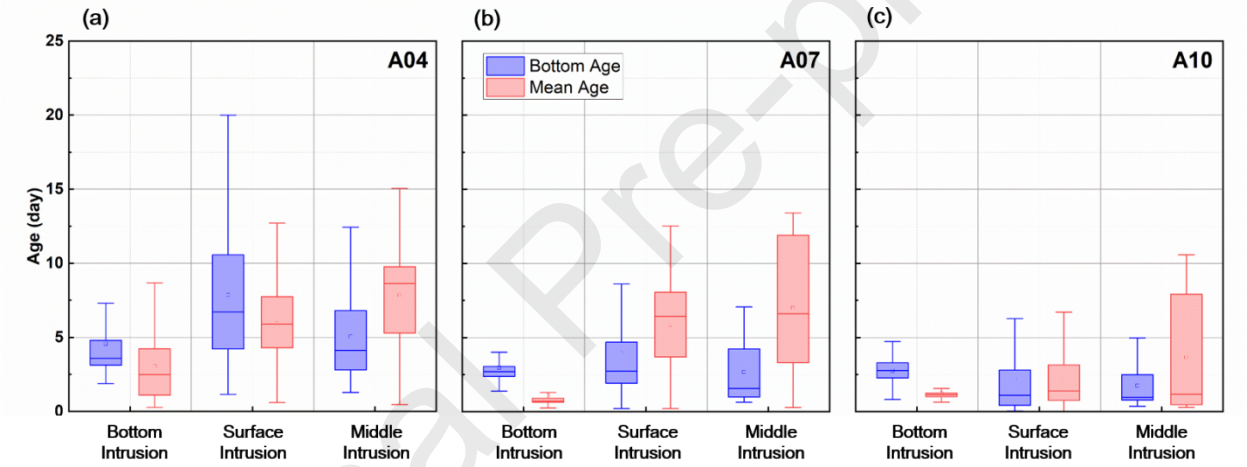

Figure 12. *VWA* under different intruding format at the (a) lower reach (A04), (b) middle reach (A07), (c) and upper reach (A10). The blue box represents the bottom *VWA* and the red box represents the depth-averaged age. The lines in the box denote mean values, the square symbols denote medians, rectangles denote the first and third quartiles, and the whiskers represent the maximum and minimum values.

4 Discussion

The calibrated and validated 3D hydrodynamic-based age model could reproduce the spatial-temporal pattern of thermal stratification and the different forms of intruding density currents, which were in line with previous studies (Ma et al., 2015, Long et al., 2019). It could also capture the special thermal structures and circulation patterns, which we believed to be the results of the integrated effects of intruding currents, upstream inflow, and stratification in the long term (seasonal scale). Furthermore, in the short term (weekly scale), the development of

these special thermal structures was also influenced by reservoir impoundment and shifts in meteorological conditions (Zhao et al., 2022; more details can be found in the SI). Our results illustrated that the *VWA* was able to characterise the vertical water renewal and integrate complex hydrodynamic processes. To the best of our knowledge, the present study is the first research which examined the vertical water renewal by adopting a vertical timescale – the *VWA* in a 3D simulation of a freshwater system. This provides an example to showcase the effectiveness and significance of *VWA*, particularly in highly dynamic systems.

4.1 The *VWA* provides additional information for vertical water exchange and biogeochemical analyses

Biogeochemical and ecological studies often rely on the commonly used thermal parameters, e.g., the MLD, thermocline thickness, thermocline strength, and thermal stability, etc., which might be too simplistic to represent the relevant hydrodynamic process in such dynamic systems as XXB. These parameters mainly focus on stratification or vertical mixing, and are not sufficient to include other processes affecting vertical transport, e.g., upstream underflow, and intruding currents from the mainstream, as observed in XXB. In our case for instance, although *VWA* increased when the MLD decreased (Figure 11), the MLD could only partly reveal the vertical water renewal: there was still old water in the epilimnion due to circulations whereas there was young water in the hypolimnion due to upstream flushing (Figure 10). Especially in the middle and lower reaches, *VWA* lay between 3 and 20 days unless the MLD approached the local maximum depth (Figure 11). Then the vertical mixing took control of *VWA* from the horizontal replacement. In other words, the water above the thermocline was not always well-mixed, and the water below the thermocline was not always poorly mixed. Although the *VWA* increased below the thermocline at most times, the mere existence of stratification may not be the direct reason for increasing *VWA* because the highest ages were observed when stratification was weak. Clearly the complex circulation patterns played a decisive role here. Existing mixed layer definitions can only distinguish the two states of stratified and unstratified, but cannot infer the rates of mixing. Moreover, although the mixed layer depth is often used in biogeochemical analyses, it can be notoriously difficult to quantify (Gray et al., 2020), and several definitions for it exist (Wilson et al., 2020). This is especially the case in riverine systems like XXB, where the complicated circulation changed the original mixing state, and the bottom water was mostly younger than the depth averaged age (Figure 12). The timescale of vertical water renewal can be a complementary hydrodynamic proxy for studying biogeochemical dynamics, and *VWA* may be more useful for this purpose because it can be compared to biogeochemical process rates. As such, the vertical water renewal rate can be represented as the inverse of the *VWA*, as a common scale in units of day^{-1}. This allows a direct comparison of some important biogeochemical rates in the same units, such as the consumption rate of dissolved oxygen (DO), or the uptake rate of carbon dioxide by phytoplankton (Shen et al., 2013, Xiong and Shen 2022, Gai et al., 2023).

4.2 Implications for hypoxia and water quality management

The development of hypoxia and anoxia is governed by net dissolved oxygen (DO) consumption (i.e., photosynthesis/respiration of phytoplankton, nitrification, mineralisation in the sediment (SOD) and water column, etc.), as well as the vertical exchange of DO by pure hydrodynamic processes. While many studies focused on the former local processes, however, quantitative investigations on the underlying pure hydrodynamic processes associated with DO in lakes and reservoirs, still needed to be further studied (Kreling et al., 2017). The definition of *VWA* in the present study is useful for characterising DO dynamics as water parcels are replenished with oxygen during contact with the atmosphere, which could well represent the DO vertical exchange process (Sun et al., 2019a). This is especially the case in dynamic systems with high water renewal relative to biogeochemical process rates. In such water bodies, vertical water renewal plays a decisive role in DO dynamics (Maes et al., 2007, Mialet et al., 2011, Azhikodan and Yokoyama 2016), and can be well reflected by *VWA*.

Monitoring the spatial-temporal distribution of DO across large reservoirs is challenging. However, in dynamic fluvial systems, assessing the risk of DO depletion might be assessable by calculating the *VWA*. Previous research (Sun et al., 2019a) estimated bottom DO using *VWA* in marine systems. Here, we reversed this approach to predict *VWA* thresholds for hypoxia and anoxia. Accordingly, hypoxia and anoxia were more likely to form in XXB when the *VWA* was over ~10 and 14 days, respectively. Therefore, during the period when *VWA* exceeded these critical values in the hypolimnion, dam operations such as enlarging water level fluctuations (Song et al., 2023b) and selective withdrawal from the upstream dam (Mi et al., 2022, Song et al., 2023a) could potentially be adopted to reduce vertical water age and mitigate hypoxia and anoxia risks. However, considering phytoplankton's role in oxygen dynamics, incorporating their effects is advised for improved DO depletion prediction with this approach, especially in productive environments.

4.3 Merits and limitations

Previous studies have stated that the traditional definition of water age, that is, the horizontal water age since entering the system, could potentially reflect the nutrient/pollutant transport and phytoplankton distribution in lakes and reservoirs since it quantifies the water exchange processes (Gao et al., 2018, Stumpner et al., 2020, Chen et al., 2022, Song et al., 2022). However, this approach is highly dependent on the definition of the upstream/downstream boundaries (Wu et al., 2017), and varies tremendously among study sites (Song 2023). Our examination of the *VWA*, focused on the vertical water renewal with fixed boundary settings (the *VWA* was set to zero at the water surface). This not only helps to evaluate the spatial-temporal distribution of vertical water renewal, but also applies to biogeochemical processes at the surface like gas exchange and the subsequent DO depletion (Sun et al., 2019a), or the transportation of surface-produced particulate organic matter (Xiong and Shen 2022). The *VWA* may also provide some insights into carbon-dioxide limitation of blooms, which can be transient yet strong, and difficult otherwise to quantify (Ibelings and Maberly 1998).

Our modelling area includes the intersection between the mainstream and tributary (Figure 1b), in order to accurately mimic the exchange processes in the intersection, e.g., the intruding currents from the Yangtze mainstream into the bay, which was an essential process in XXB. The flows at the intersection possess significant 3D hydrodynamic characteristics (figure S4), which could not be properly simulated by a lower dimensional model. In addition, the vertical grids we used were structured z-coordinates, which were more appropriate for inland waters due to the steep bed slope, while the vertical grids of the oceanography studies applying similar approach are σ-coordinates. This also means the code we modified was very different from the perspective of technical concerns.

Nevertheless, there are limitations to the current technique. First, although the *VWA* serves as a valuable hydrodynamic indicator in dynamic systems, particularly where intrusion affects the circulation like in XXB, the widespread applicability of *VWA* in other surface water systems remains unclear. This is because the MLD is easy to calculate and more versatile since there are multiple approaches to define it, e.g. using temperature profiles, or eddy diffusivity. Moreover, 3D hydrodynamic modelling may not be feasible in some cases, and it may not be necessary in water systems without intrusion phenomena. Consequently, the applicability and generalizability of *VWA* are recommended to be further explored in various lentic waterbodies. Second, although our definition of *VWA* is directly relevant for physical-biological processes like DO depletion and particulate organic matter transportation, it cannot directly explain the phytoplankton occurring at the surface because the age value is forced to be zero at the surface boundary. Nevertheless, phytoplankton blooms can be characterized by either surface concentrations (e.g., Sverdrup (1953)) or depth-integrated concentrations (e.g., Behrenfeld (2010)), representing elevated phytoplankton levels in the surface water and throughout the water column, respectively (Berman and Gildor 2022). Future studies investigating the relationship between the depth-integrated phytoplankton concentrations and the *VWA* within the euphotic zone are recommended. Lastly, due to the limitation in the spatial-temporal resolution of *in situ* observations, our model was only calibrated and validated using a dataset covering several months over one year. Thus, some rapid variations of hydrodynamic processes in shorter time scales may not be fully captured. For future modelling approach, we recommend conducting high resolution monitoring (Kong et al., 2020), for improving the precision and function of the model.

5 Conclusions

In this study, we implemented a technique based on the vertical timescale – *VWA* – to quantify the vertical water renewal in XXB and associated it with water environment and management issues. The results of our 3D hydrodynamic-based age model showed that the special thermal structures were mainly caused by stratification and intruding density currents from the mainstream in the long term and by the impoundment process and changes in air temperature and wind in the short term. The vertical renewal characterized by age displayed

significant spatial patterns and seasonal variations. *VWA* was large in spring and summer, and small in autumn and winter, with a maximum of 25 days in April when water entered from TGD main basin at mid depth. During the period when mainstream water intruded from the bottom, the vertical water renewal was considerably faster than the middle and surface intrusion periods. One of the most significant findings was that there was still old water in the surface waters due to circulations and young water above the river bed due to upstream flushing. Furthermore, the bottom vertical renewal was usually faster than the depth-averaged vertical renewal (50% faster especially during middle intruding period), which had rarely been encountered in natural lakes. These findings indicated the commonly used thermal parameters like the MLD are insufficient to represent the entire vertical exchange process. Based on the quantification of vertical renewal, we predicted that hypoxia and anoxia were more likely to develop in XXB when the *VWA* exceeded ~10 and 14 days, respectively. The application of *VWA* offers a new approach to compare the physical transport timescale with the timescales for biogeochemical processes. Furthermore, it may provide an auxiliary indicator to guide dam operation and alleviate the risk of hypoxia and anoxia and other environmental issues.

Acknowledgements

This research is supported by the National Key R&D Program of China (2022YFC3202700), Guangxi Science and Technology Major Project (No. AA23023009), and the National Natural Science Foundation of China (U2243238, 12002332). B. Gai is additionally supported by the China Scholarship Council (CSC), and the Helmholtz-Centre for Environmental Research (UFZ) program integration budget. The authors are grateful to the funding institutions for their support. Finally, we appreciate the editor and three anonymous reviewers for their invaluable comments and suggestions to improve the manuscript.

References

Akiyama, J. and Stefan, H.G., 1984. Plunging Flow into a Reservoir: Theory. Journal of Hydraulic Engineering 10(4), 484-499.

Ayala, A.I., Cortés, A., Fleenor, W.E. and Rueda, F.J., 2014. Seasonal scale modeling of river inflows in stratified reservoirs: Structural vs. parametric uncertainty in inflow mixing. Environmental Modelling & Software 60, 84-98. https://dx.doi.org/10.1016/j.envsoft.2014.06.011.

Azhikodan, G. and Yokoyama, K., 2016. Spatio-temporal variability of phytoplankton (Chlorophyll-a) in relation to salinity, suspended sediment concentration, and light intensity in a macrotidal estuary. Continental Shelf Research 126, 15-26.

Behrenfeld, M.J., 2010. Abandoning Sverdrup's Critical Depth Hypothesis on phytoplankton blooms. Ecology 91(4), 977-989. https://dx.doi.org/10.1890/09-1207.1.

Berman, H. and Gildor, H., 2022. Phytoplankton Bloom in the Gulf of Elat/Aqaba: Physical Versus Ecological Forcing. Journal of Geophysical Research: Oceans 127(5). https://dx.doi.org/10.1029/2021jc017922.

Bocaniov, S.A., Lamb, K.G., Liu, W., Rao, Y.R. and Smith, R.E.H., 2020. High Sensitivity of Lake Hypoxia to Air Temperatures, Winds, and Nutrient Loading: Insights From a 3-D Lake Model. Water Resources Research 56(12). https://dx.doi.org/10.1029/2019wr027040.

Bocaniov, S.A. and Scavia, D., 2018. Nutrient Loss Rates in Relation to Transport Time Scales in a Large Shallow Lake (Lake St. Clair, USA—Canada): Insights From a Three-Dimensional Model. Water Resources Research 54(6), 3825-3840. https://dx.doi.org/10.1029/2017wr021876.

Boehrer, B., von Rohden, C. and Schultze, M., 2017. Ecology of Meromictic Lakes, pp. 15-34.

Cai, H., Piccolroaz, S., Huang, J., Liu, Z., Liu, F. and Toffolon, M., 2018. Quantifying the impact of the Three Gorges Dam on the thermal dynamics of the Yangtze River. Environmental Research Letters 13(5). https://dx.doi.org/10.1088/1748-9326/aab9e0.

Chen, M., You, L.-H., Zhang, L.-L., Liao, N., Song, Y., Wang, H.-W. and Li, J., 2022. Mixing processes in a reservoir corresponding to different water level operations caused spatial differences during two phytoplankton bloom events. Journal of Hydrology 612. https://dx.doi.org/10.1016/j.jhydrol.2022.128139.

Chuo, M., Ma, J., Liu, D. and Yang, Z., 2019. Effects of the impounding process during the flood season on algal blooms in Xiangxi Bay in the Three Gorges Reservoir, China. Ecological Modelling 392, 236-249. https://dx.doi.org/10.1016/j.ecolmodel.2018.11.017.

Curtis, R.G., Needoba, J.A., Baptista, A.M. and A?El, J.A., 2011. Coastal Upwelling Supplies Oxygen-Depleted Water to the Columbia River Estuary. PLoS One 6(4), e18672.

de Boyer Montégut, C., 2004. Mixed layer depth over the global ocean: An examination of profile data and a profile-based climatology. Journal of Geophysical Research 109(C12). https://dx.doi.org/10.1029/2004jc002378.

de Brye, B., de Brauwere, A., Gourgue, O., Delhez, E.J. and Deleersnijder, E., 2012. Water renewal timescales in the Scheldt Estuary. Journal of Marine Systems 94, 74-86.

Deleersnijder, E., Campin, J.-M. and Delhez, E.J., 2001. The concept of age in marine modelling: I. Theory and preliminary model results. Journal of Marine Systems 28(3-4), 229-267.

Delhez, E., Campin, J.M., Hirst, A.C. and Deleersnijder, E., 1999. Toward a general theory of the age in ocean modelling. Ocean Modelling 1(1), 17-27.

Delhez, E.J.M. and Deleersnijder, R., 2002. The concept of age in marine modelling. Journal of Marine Systems 31(4), 279-297.

Deltares, 2013. Delft3D-FLOW user mannual. The Netherlands, Delft Hydraulics.

Dong, F., Mi, C., Hupfer, M., Lindenschmidt, K.E., Peng, W., Liu, X. and Rinke, K., 2019. Assessing vertical diffusion in a stratified lake using a three-dimensional hydrodynamic model. Hydrological Processes 34(5), 1131-1143. https://dx.doi.org/10.1002/hyp.13653.

Ezer, T. and Mellor, G.L., 2004. A generalized coordinate ocean model and a comparison of the bottom boundary layer dynamics in terrain-following and in z-level grids. Ocean Modelling 6(3-4), 379-403. https://dx.doi.org/10.1016/s1463-5003(03)00026-x.

Gai, B., Sun, J., Lin, B., Li, Y., Mi, C. and Shatwell, T., 2023. Vertical mixing and horizontal transport unravel phytoplankton blooms in a large riverine reservoir. Journal of Hydrology 627. https://dx.doi.org/10.1016/j.jhydrol.2023.130430.

Gao, Q., He, G., Fang, H., Bai, S. and Huang, L., 2018. Numerical simulation of water age and its potential effects on the water quality in Xiangxi Bay of Three Gorges Reservoir. Journal of Hydrology.

Goede, E.D.D., 2020. Historical overview of 2D and 3D hydrodynamic modelling of shallow water flows in the Netherlands. Ocean Dynamics 70(2).

Gourgue, O., Deleersnijder, E. and White, L., 2007. Toward a generic method for studying water renewal, with application to the epilimnion of Lake Tanganyika. Estuarine Coastal and Shelf Science 74(4), 764-776.

Gray, E., Mackay, E.B., Elliott, J.A., Folkard, A.M. and Jones, I.D., 2020. Wide-spread inconsistency in estimation of lake mixed depth impacts interpretation of limnological processes. Water Res 168, 115136. https://dx.doi.org/10.1016/j.watres.2019.115136.

Holbach, A., Norra, S., Wang, L., Yuan, Y., Wei, H., Zheng, B. and Bi, Y., 2014. Three Gorges Reservoir: Density Pump Amplification of Pollutant Transport into Tributaries. Environmental Science & Technology 48(14), 7798-7806.

Horn, C., Metzler, P., Ullrich, K., Koschorreck, M. and Boehrer, B., 2017. Methane storage and ebullition in monimolimnetic waters of polluted mine pit lake Vollert-Sued, Germany. Sci Total Environ 584-585, 1-10. https://dx.doi.org/10.1016/j.scitotenv.2017.01.151.

Ibelings, B.W. and Maberly, S.C., 1998. Photoinhibition and the availability of inorganic carbon restrict photosynthesis by surface blooms of cyanobacteria. Limnology and Oceanography 43(3), p.408-419.

Ji, D.B., Fang, J., long, L.H., Yang, Z.J., Zhao, X.X., Yang, X. and Guo, Y.L., 2022. Characteristics and Differences of Dissolved Oxygen Stratification on Different Tributaries of Three Gorges Reservoir During Impoundment Period. Environmental Science 43(7), 9.

Ji, D.B., Wells, S.A., Yang, Z.J., Liu, D.F., Huang, Y.L., Ma, J. and Berger, C.J., 2017. Impacts of water level rise on algal bloom prevention in the tributary of Three Gorges Reservoir, China. Ecological Engineering 98, 70-81. https://dx.doi.org/10.1016/j.ecoleng.2016.10.019.

Kärnä, T. and Baptista, A.M., 2016. Water age in the Columbia River estuary. Estuarine, Coastal and Shelf Science 183, 249-259.

Köhler, J., Wang, L., Guislain, A. and Shatwell, T., 2018. Influence of vertical mixing on light-dependency of phytoplankton growth. Limnology and Oceanography 63(3), 1156-1167. https://dx.doi.org/10.1002/lno.10761.

Kong, X., Seewald, M., Dadi, T., Friese, K., Mi, C., Boehrer, B., Schultze, M., Rinke, K. and Shatwell, T., 2020. Unravelling winter diatom blooms in temperate lakes using high frequency data and ecological modeling. Water Research. https://dx.doi.org/10.1016/j.watres.2020.116681.

Kreling, J., Bravidor, J., Engelhardt, C., Hupfer, M., Koschorreck, M. and Lorke, A., 2017. The importance of physical transport and oxygen consumption for the development of a metalimnetic oxygen minimum in a lake. Limnology and Oceanography 62(1), 348-363. https://dx.doi.org/10.1002/lno.10430.

Kwak, M.T. and Cho, Y.K., 2019. Seasonal Variation in Residence Times of Two Neighboring Bays with Contrasting Topography. Estuaries and Coasts (5).

Lewis, W.M., McCutchan, J.H. and Roberson, J., 2019. Effects of Climatic Change on Temperature and Thermal Structure of a Mountain Reservoir. Water Resources Research 55(3), 1988-1999. https://dx.doi.org/10.1029/2018wr023555.

Li, X., Liu, B., Wang, Y., Yang, Y., Liang, R., Peng, F., Xue, S., Zhu, Z. and Li, K., 2020a. Hydrodynamic and environmental characteristics of a tributary bay influenced by backwater jacking and intrusions from a main reservoir. Hydrology and Earth System Sciences 24(11), 5057-5076. https://dx.doi.org/10.5194/hess-24-5057-2020.

Li, Y., Sun, J., Lin, B. and Liu, Z., 2020b. Thermal-hydrodynamic circulations and water fluxes in a tributary bay of the Three Gorges Reservoir. Journal of Hydrology 585. https://dx.doi.org/10.1016/j.jhydrol.2019.124319.

Liu, D., Huang, Y. and Ji, D., 2013. Algal blooms and ecological regulation in tributaries of Three Gorges Reservoir China Water Resources and Hydropower Press.

Liu, L., Liu, D., Johnson, D.M., Yi, Z. and Huang, Y., 2012. Effects of vertical mixing on phytoplankton blooms in Xiangxi Bay of Three Gorges Reservoir: Implications for management. Water Research 46(7), 2121-2130. https://dx.doi.org/10.1016/j.watres.2012.01.029.

Liu, W., Bocaniov, S.A., Lamb, K.G. and Smith, R.E.H., 2014. Three dimensional modeling of the effects of changes in meteorological forcing on the thermal structure of Lake Erie. Journal of great lakes research 40(4), 827-840. https://dx.doi.org/10.1016/j.jglr.2014.08.002.

Long, L., Ji, D., Liu, D., Yang, Z. and Lorke, A., 2019. Effect of Cascading Reservoirs on the Flow Variation and Thermal Regime in the Lower Reaches of the Jinsha River. Water 11(5). https://dx.doi.org/10.3390/w11051008.

Ma, J., Liu, D., Wells, S.A., Tang, H., Ji, D. and Yang, Z., 2015. Modeling density currents in a typical tributary of the Three Gorges Reservoir, China. Ecological Modelling 296, 113-125. https://dx.doi.org/10.1016/j.ecolmodel.2014.10.030.

Maes, J., Stevens, M. and Breine, J., 2007. Modelling the migration opportunities of diadromous fish species along a gradient of dissolved oxygen concentration in a European tidal watershed. Estuarine, Coastal and Shelf Science 75(1-2), 151-162.

Mao, J., Jiang, D. and Dai, H., 2015. Spatial–temporal hydrodynamic and algal bloom modelling analysis of a reservoir tributary embayment. Journal of Hydro-environment Research 9(2), 200-215. https://dx.doi.org/https://doi.org/10.1016/j.jher.2014.09.005.

McCullough, G.K., Barber, D. and Cooley, P.M., 2007. The Vertical Distribution of Runoff and its Suspended Load in Lake Malawi. Journal of great lakes research 33(2), 449-465. https://dx.doi.org/https://doi.org/10.3394/0380-1330(2007)33[449:TVDORA]2.0.CO;2.

Mi, C., Hamilton, D.P., Frassl, M.A., Shatwell, T., Kong, X., Boehrer, B., Li, Y., Donner, J. and Rinke, K., 2022. Controlling blooms of Planktothrix rubescens by optimized metalimnetic water withdrawal: a modelling study on adaptive reservoir operation. Environmental Sciences Europe 34(1). https://dx.doi.org/10.1186/s12302-022-00683-3.

Mialet, B., Gouzou, J., Azémar, F., Maris, T., Sossou, C., Toumi, N., Van Damme, S., Meire, P. and Tackx, M., 2011. Response of zooplankton to improving water quality in the Scheldt estuary (Belgium). Estuarine, Coastal and Shelf Science 93(1), 47-57.

Ministry of Environmental Protection of China, L., 2014. Bulletin on the ecological and environmental monitoring results of the TGP (2003-2013).

Muller, B., Bryant, L.D., Matzinger, A. and Wuest, A., 2012. Hypolimnetic oxygen depletion in eutrophic lakes. Environ Sci Technol 46(18), 9964-9971. https://dx.doi.org/10.1021/es301422r.

O'Brien, K.R., Burford, M.A. and Brookes, J.D., 2009. Effects of light history on primary productivity in a phytoplankton community dominated by the toxic cyanobacteriumCylindrospermopsis raciborskii. Freshwater Biology 54(2), 272-282. https://dx.doi.org/10.1111/j.1365-2427.2008.02106.x.

Qin, Z., 1980. A contribution to the calculation of wind stress on sea surface. Trans Oceanology Limn 3, 1-8.

Shatwell, T., Nicklisch, A. and Köhler, J., 2012. Temperature and photoperiod effects on phytoplankton growing under simulated mixed layer light fluctuations. Limnology and Oceanography 57(2), 541-553. https://dx.doi.org/10.4319/lo.2012.57.2.0541.

Shen, J., Hong, B. and Kuo, A.Y., 2013. Using timescales to interpret dissolved oxygen distributions in the bottom waters of Chesapeake Bay. Limnology & Oceanography 58(6), 2237-2248.

Shi, L., Sun, J., Lin, B., Liu, Z. and Zuo, X., 2022. Hydro-Thermodynamic Processes at a Large Confluence Under Reservoir Regulation. Water Resources Research 58(12), e2022WR033315. https://dx.doi.org/https://doi.org/10.1029/2022WR033315.

Song, Y., 2023. Hydrodynamic impacts on algal blooms in reservoirs and bloom mitigation using reservoir operation strategies: A review. Journal of Hydrology 620. https://dx.doi.org/10.1016/j.jhydrol.2023.129375.

Song, Y., Chen, M., Li, J., Zhang, L., Deng, Y. and Chen, J., 2023a. Can selective withdrawal control algal blooms in reservoirs? The underlying hydrodynamic mechanism. Journal of Cleaner Production 394, 136358. https://dx.doi.org/https://doi.org/10.1016/j.jclepro.2023.136358.

Song, Y., Shen, L., Zhang, L., Li, J. and Chen, M., 2021a. Study of a hydrodynamic threshold system for controlling dinoflagellate blooms in reservoirs. Environ Pollut 278, 116822. https://dx.doi.org/10.1016/j.envpol.2021.116822.

Song, Y., Shen, L., Zhang, L.L., Li, J. and Chen, M., 2021b. Study of a hydrodynamic threshold system for controlling dinoflagellate blooms in reservoirs. Environmental Pollution 278. https://dx.doi.org/10.1016/j.envpol.2021.116822.

Song, Y., You, L., Chen, M., Li, J., Zhang, L. and Peng, T., 2022. Key hydrodynamic principles for controlling algal blooms using emergency reservoir operation strategies. J Environ Manage 325(Pt A), 116470. https://dx.doi.org/10.1016/j.jenvman.2022.116470.

Song, Y., You, L.H., Chen, M., Li, J., Zhang, L.L. and Peng, T., 2023b. Key hydrodynamic principles for controlling algal blooms using emergency reservoir operation strategies. Journal of Environmental Management 325. https://dx.doi.org/10.1016/j.jenvman.2022.116470.

Stephens, G.L., Slingo, J.M., Rignot, E., Reager, J.T., Hakuba, M.Z., Durack, P.J., Worden, J. and Rocca, R., 2020. Earth's water reservoirs in a changing climate. Proceedings of the Royal Society A 476(2236), 20190458.

Stumpner, E.B., Bergamaschi, B.A., Kraus, T.E., Parker, A.E., Wilkerson, F.P., Downing, B.D., Dugdale, R.C., Murrell, M.C., Carpenter, K.D. and Orlando, J.L., 2020. Spatial variability of phytoplankton in a shallow tidal

freshwater system reveals complex controls on abundance and community structure. Science of The Total Environment 700, 134392.

Sun, J., Liu, L., Lin, J., Lin, B. and Zhao, H., 2019a. Vertical water renewal in a large estuary and implications for water quality. Sci Total Environ, 135593. https://dx.doi.org/10.1016/j.scitotenv.2019.135593.

Sun, J., Zhou, J., Zhang, M. and Lin, B., 2019b. Investigation on hydrothermal processes in a large channel-type reservoir using an integrated physics-based model. Journal of Hydroinformatics 21(3), 493-509. https://dx.doi.org/10.2166/hydro.2019.139.

Sverdrup, 1953. On conditions for the vernal blooming of phytoplanktopn. ICES Journal of Marine Science 18(3), 287-295.

Tang, C., He, C., Li, Y. and Acharya, K., 2021. Diverse responses of hydrodynamics, nutrients and algal biomass to water diversion in a eutrophic shallow lake. Journal of Hydrology 593. https://dx.doi.org/10.1016/j.jhydrol.2020.125933.

Wentzky, V.C., Frassl, M.A., Rinke, K. and Boehrer, B., 2019. Metalimnetic oxygen minimum and the presence of Planktothrix rubescens in a low-nutrient drinking water reservoir. Water Res 148, 208-218. https://dx.doi.org/10.1016/j.watres.2018.10.047.

Wilson, H.L., Ayala, A.I., Jones, I.D., Rolston, A., Pierson, D., de Eyto, E., Grossart, H.-P., Perga, M.-E., Woolway, R.I. and Jennings, E., 2020. Variability in epilimnion depth estimations in lakes. Hydrology and Earth System Sciences. https://dx.doi.org/10.5194/hess-2020-222.

Wu, B., Wang, G., Wang, Z., Liu, C. and Ma, J., 2017. Integrated hydrologic and hydrodynamic modeling to assess water exchange in a data-scarce reservoir. Journal of Hydrology 555, 15-30. https://dx.doi.org/10.1016/j.jhydrol.2017.09.057.

Xiong, J. and Shen, J., 2022. Vertical Transport Timescale of Surface-Produced Particulate Material in the Chesapeake Bay. Journal of Geophysical Research: Oceans 127(2). https://dx.doi.org/10.1029/2021jc017592.

Xu, H., Yan, M., Long, L., Ma, J., Ji, D., Liu, D. and Yang, Z., 2021. Modeling the Effects of Hydrodynamics on Thermal Stratification and Algal Blooms in the Xiangxi Bay of Three Gorges Reservoir. Frontiers in Ecology and Evolution 8. https://dx.doi.org/10.3389/fevo.2020.610622.

Yang, R., Wu, S., Wu, X., Ptak, M., Li, X., Sojka, M., Graf, R., Dai, J. and Zhu, S., 2022a. Quantifying the impacts of climate variation, damming, and flow regulation on river thermal dynamics: a case study of the Włocławek Reservoir in the Vistula River, Poland. Environmental Sciences Europe 34(1). https://dx.doi.org/10.1186/s12302-021-00583-y.

Yang, Z., Wei, C., Liu, D., Lin, Q., Huang, Y., Wang, C., Ji, D., Ma, J. and Yang, H., 2022b. The influence of hydraulic characteristics on algal bloom in Three Gorges Reservoir, China: A combination of cultural experiments and field monitoring. Water Research. https://dx.doi.org/10.1016/j.watres.2021.118030.

Yang, Z., Xu, P., Liu, D., Ma, J., Ji, D. and Cui, Y., 2018. Hydrodynamic mechanisms underlying periodic algal blooms in the tributary bay of a subtropical reservoir. Ecological Engineering 120, 6-13. https://dx.doi.org/10.1016/j.ecoleng.2018.05.003.

Zhang, H., Shen, Y. and Tang, J., 2021. Hydrodynamics and water renewal in the Pearl River Estuary, China: A numerical study from the perspective of water age. Ocean Engineering 237. https://dx.doi.org/10.1016/j.oceaneng.2021.109639.

Zhao, X., Yang, Z., Ji, D., Long, L., Yang, Z., Xu, H., Cheng, Z. and Liu, D., 2022. Meteorological forcing and hydrological connectivity together control the thermal regime of Xiangxi Bay, a tributary of the Three Gorges Reservoir. Journal of Hydrology 612. https://dx.doi.org/10.1016/j.jhydrol.2022.128276.

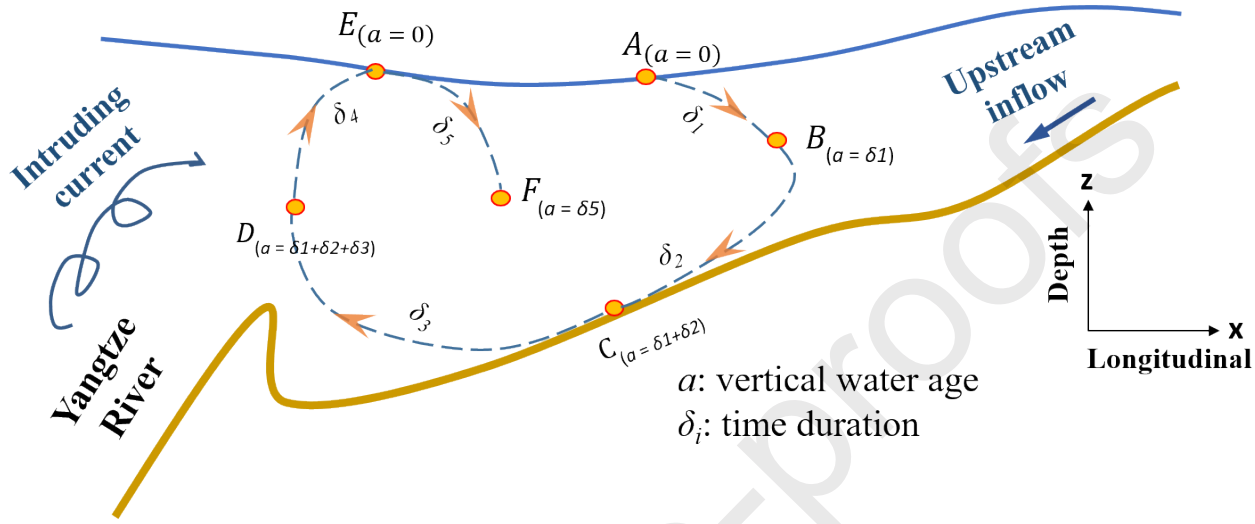

Highlights:

- Vertical water age (*VWA*) was first simulated in lentic systems to quantify water renewal.
- Vertical water renewal mainly depends on stratification and forms of intruding density currents.
- Bottom water was often younger than overlying intermediate waters due to intrusion.
- *VWA* serves as a helpful proxy for water quality issues in dynamic systems.